symmetry

MDPI

Article

A Promising Glass Type in Electronic and Laser Applications: Elastic Moduli, Mechanical, and Photon Transmission Properties of WO_3 Reinforced Ternary-Tellurite Glasses

Ghada ALMisned [1], Elaf Rabaa [2], Yasser S. Rammah [3], Ziad Y. Khattari [4], Duygu Sen Baykal [5], Erkan Ilik [6], Gokhan Kilic [6], Hesham M. H. Zakaly [7,8], Antoaneta Ene [9,*] and Huseyin Ozan Tekin [2,10,*]

1 Department of Physics, College of Science, Princess Nourah Bint Abdulrahman University, P.O. Box 84428, Riyadh 11671, Saudi Arabia
2 Medical Diagnostic Imaging Department, College of Health Sciences, University of Sharjah, Sharjah 27272, United Arab Emirates
3 Department of Physics, Faculty of Science, Menoufia University, Shebin El-Koom, Menoufia 32511, Egypt
4 Department of Physics, Faculty of Science, The Hashemite University, P.O. Box 330127, Zarqa 13133, Jordan
5 Medical Imaging Techniques, Vocational School of Health Sciences, Istanbul Kent University, Istanbul 34433, Turkey
6 Department of Physics, Faculty of Science, Eskisehir Osmangazi University, Eskisehir 26040, Turkey
7 Institute of Physics and Technology, Ural Federal University, 620002 Ekaterinburg, Russia
8 Physics Department, Faculty of Science, Al-Azhar University, Assiut 71524, Egypt
9 INPOLDE Research Center, Department of Chemistry, Physics and Environment, Faculty of Sciences and Environment, Dunarea de Jos University of Galati, 47 Domneasca Street, 800008 Galati, Romania
10 Computer Engineering Department, Faculty of Engineering and Natural Sciences, Istinye University, Istanbul 34396, Turkey
* Correspondence: antoaneta.ene@ugal.ro (A.E.); tekin765@gmail.com or htekin@sharjah.ac.ae (H.O.T.)

check for updates

Citation: ALMisned, G.; Rabaa, E.; Rammah, Y.S.; Khattari, Z.Y.; Baykal, D.S.; Ilik, E.; Kilic, G.; Zakaly, H.M.H.; Ene, A.; Tekin, H.O. A Promising Glass Type in Electronic and Laser Applications: Elastic Moduli, Mechanical, and Photon Transmission Properties of WO_3 Reinforced Ternary-Tellurite Glasses. *Symmetry* **2023**, *15*, 602. https://doi.org/10.3390/sym15030602

Academic Editors: Sergei D. Odintsov, Raffaele Barretta and Tomohiro Inagaki

Received: 29 January 2023
Revised: 14 February 2023
Accepted: 24 February 2023
Published: 27 February 2023

Abstract: We report the symmetry of mechanical and gamma-ray attenuation properties for some tellurite glasses through elastic moduli, mechanical, and transmission properties as a function of varied WO_3 amount in glass configuration. Four glass samples, along with different molar compositions as well as WO_3/GdF3 substitution ratios, are investigated. Transmission properties using several essential parameters, such as attenuation coefficients, half-value layers, effective atomic numbers, effective conductivity, and buildup factors, are calculated in the 0.015–15 MeV energy range. Moreover, elastic moduli and Poisson's ratios (σ) of the studied glass are calculated using the Makishima–Mackenzie model. The M4 sample with the highest WO_3 addition is found with superior photon attenuation properties among the glasses investigated. Poisson's ratio (σ) is increased, while all elastic moduli are decreased. Young's modulus is reported as 62.23 GPa and 36.45.37 GPa at the highest and lowest WO_3 mol%, respectively. It can be concluded that WO_3 is a functional and monotonic tool in ternary-tellurite glasses for multiple modifications and enhancement purposes on gamma-ray attenuation, elastic moduli, and mechanical properties. It can also be concluded that increasing the WO_3 amount in tellurite glasses may be considered a tool in terms of providing symmetry for mechanical and gamma-ray attenuation properties.

Keywords: tellurite glasses; mechanical properties; elastic moduli; attenuation; radiation shielding

1. Introduction

Since ionizing radiation has become widely used medical, scientific, and industrial applications, it is mandatory to enhance the protection methods against its hazards to living biological tissues and eventually public health [1,2]. Ionizing radiations namely alpha, beta, gamma-ray, and X-ray, can cause health effects to a certain degree depending on the type and the amount of energy being absorbed. As the dose a person receives increases, the risk of having health effects increases Because of its ability to alter cell structure and damage genetic information, radiation is known to have both immediate and long-term

harmful consequences for living cells, including increased risk of congenital anomalies and cancer through DNA modifications [3–5]. The impact of ionizing radiation comes either from exposure to a large amount at once or after years of being exposed to a constant radiation source, as the probability of cancer or a genetic effect occurring may increase. Ionizing radiation is widely used in medical fields for various applications, including diagnostic imaging, radiation therapy, and medical research [6–8]. Thus, several shielding materials, such as aprons and gloves, have been developed to protect patients and medical staff from direct and secondary radiation exposure [9]. Generally, the shielding material is made from lead (Pb) due to its high density and corrosion resistance or from lead-composition materials, in which lead is mixed with other heavy materials that attenuate radiation, such as rubber, tin, and PCV vinyl [10]. However, advanced shielding material technology no longer employs non-Pb or Pb-free shielding materials because of their drawbacks of being toxic and heavy [11,12]. However, similar properties of Pb-based shielding material are achieved by mixing various additives, including tin, antimony, bismuth, and tungsten, with heavy metals that deliver the same attenuating and blocking radiation [13]. Glass system materials have captured the interest of many researchers because of their special properties, including transparency, high thermal and chemical stability, non-toxicity, and ease of fabrication [14]. In this research, we selected the tellurite glass system, as it has received more attention for its promising features as a potential substance for laser, fiber, as well as non-linear optical-devices by means of its extended infrared transmission, high gain density, low-melting temperature, and high dielectric constant [15]. Mainly, TeO_2 requires a secondary component to form glass, unlike classic glass-forming oxide. For this purpose, we chose WO_3 as our second ingredient, which would make it ideal for ensuring anti-crystallization and maintaining high density and its refractive index, as it would also extend the glass transition temperature [16]. Because of their complementary properties, fluoride and heavy metal oxide are a great fit with our third component, GdF_3, for use in mid-infrared fiber lasers and non-linear optics [17]. This research aims to investigate the gamma-ray absorption parameters of tellurite [18] glasses with different WO_3 and GdF_3 additive ratios and to investigate these parameters within the framework of a relationship with their chemical compositions. Therefore, some glasses with molar ratios given in Table 1 are extensively evaluated, and some critical gamma-ray absorption parameters are calculated. There are other studies that are similar to glass density changes in the literature. Similar findings have been observed in the density fluctuations of glasses generated as a consequence of the WO_3/Gd_2O_3 exchange [19]. To promote efficient radiation shielding material properties within the current glass composition, investigations of radiation shielding factors are conducted as a function of changing WO_3 incorporation.

Table 1. Sample densities with mole fractions.

Sample	% mol Fraction			Density (g/cm^3)
	TeO_2	WO_3	GdF_3	
M1	60	40	0	5.6824
M2	60	30	10	5.6983
M3	60	20	20	5.7705
M4	60	10	30	5.8204

2. Material and Methods

The fundamental gamma-ray shielding parameters of four distinct glass samples based on TeO_2–WO_3–GdF_3 have been reported. Previously, M1, M2, M3, and M4 glass samples were synthesized by employing the conventional process of melt-quenching [18]. Gamma-ray absorption properties have been investigated and analyzed using Py-MLBUF [20] calculation software, where they were observed in 0.015–15 MeV energy range. Thereafter,

ORIGIN was used to display the gamma-ray absorption features. The relationship between energy and parameters such as density, linear attenuation coefficient, mass attenuation coefficient, and half-value thickness were investigated. Moreover, base computations were carried out in the range of 0.015–15 MeV across a broad variety of mean free path values, covering from 0.5 mfp to 40 mfp. To determine the most efficient sample with optimal radiation shielding properties, we investigate the gamma-ray properties and mechanical properties using various theoretical and computational methods.

3. Result and Discussion

3.1. Gamma-ray Attenuation Properties

The low-to-high energy gamma-ray absorption characteristics of four different glass samples from the TeO_2–WO_3–GdF_3 glass system were examined. The glass density (g/cm^3) plays a critical role in absorbing gamma rays. Materials having a high density have a large number of atoms and electrons per unit volume; as a result, they tend to absorb more gamma and X-ray radiation because of their internal interaction with the incoming radiation. Figure 1a displays the varying densities [18] of the four synthesized samples, where the M4 sample, which contains 60 mol% of TeO_2 and 40 mol% of WO_3, shows to have the highest density value at 5.8204 g/cm^3. Adding a large proportion of WO_3 to the glass sample increased the gamma radiation absorption characteristic by increasing the glass's density.

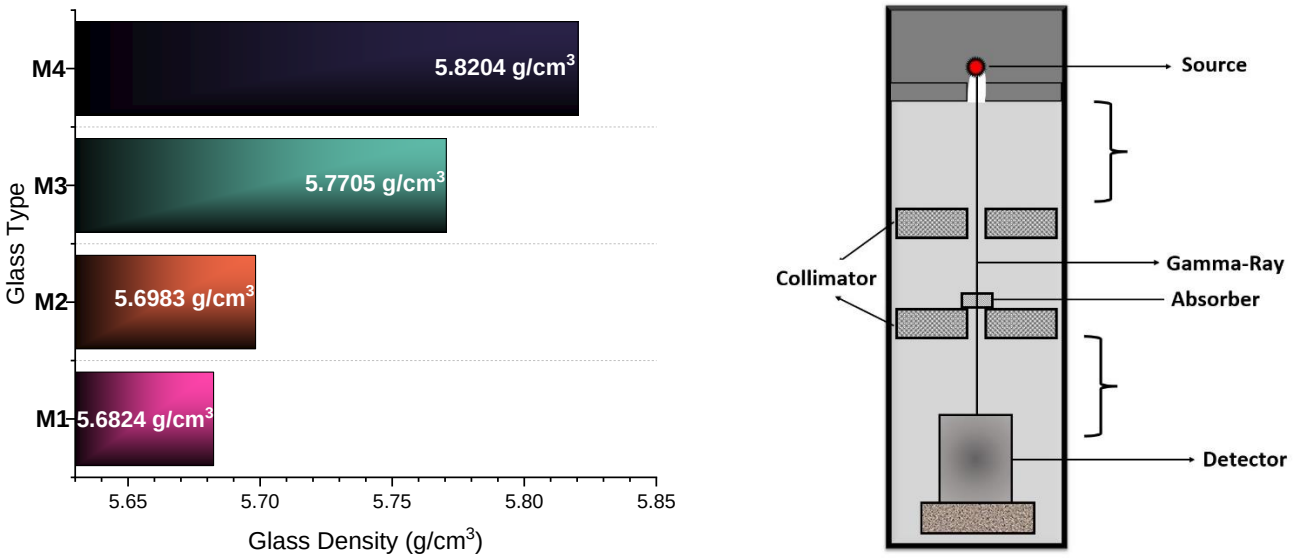

Figure 1. Variation of investigated glass densities.

For gamma-ray absorption, we calculated both the linear and mass attenuation coefficients across a broad energy range (i.e., 0.015–15 MeV). The factor that affects an absorber material's linear attenuation coefficient is its density (g/cm^3). The equation below, often known as the Beer–Lamber equation, may be used to get this quantity.

$$I = I_0 \cdot e^{-\mu x} \quad (1)$$

In which; I_0 is the incident beam intensity, I is the transmitted intensity after the beam has traveled a distance x (cm), and is the absorption coefficient (cm^{-1}) of the absorber specimen [21]. As a function of x and μ values, the intensity of I may change during the transmission process. This relationship is shown in Figure 1b. Meanwhile, Figure 2 displays the behavior of each glass sample in terms of the linear attenuation coefficient (μ) as a function of increasing the energy. As it explains, the attitude of the incident photon after

interaction with the material was fully absorbed by the electrons on the atom's orbit, or it was partially absorbed, and the rest was dispersed. It shows that high attenuation values dropped in the low energy zone, where the photoelectric effect was predominated. The graph shows a steady decrease in the high energy levels between 0.05 MeV and 6 MeV as the influence of Compton scattering grows with increasing energy. Despite the inclines and declines, the M4 sample, with the greatest concentration of WO_3, demonstrated the highest μ at practically all energy levels compared to the other samples. However, it was shown that the increased addition of WO_3 doping in the tellurite glass also influenced the linear attenuation characteristics. In addition, HVL played an essential role in the gamma-ray absorption material investigation. HVL is the minimum thickness of a material needed to decrease the intensity of an incoming photon by half; as long as the thickness of the material stays small, the efficiency of the material is confirmed to attenuate energy more effectively [22].

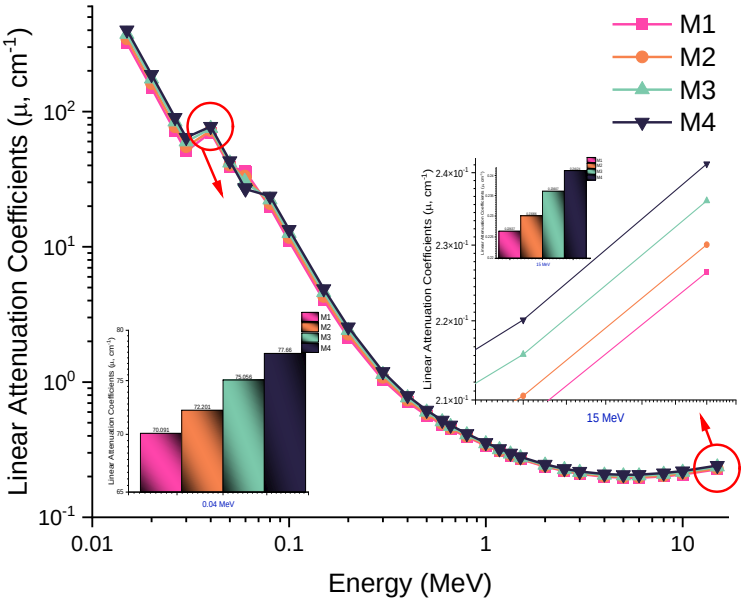

Figure 2. Variation of linear attenuation coefficient (cm^{-1}) with photon energy (MeV) for all M1–M4 glasses.

Figure 3 represents the four glass samples' HVL values as functions of energy; as the energy of the incoming photon increases, the values of HVL increase. The M4 sample, with the highest value of WO_3, exhibited the lowest HVL value of 1.33 cm at 0.6 MeV of energy, while M1, M2, and M3 had HVL values of 1.4306 cm, 1.4031 cm, and 1.3632 cm. The M4 sample was clearly superior to the other samples, making it the most efficient material for attenuating gamma radiation with the thinnest total thickness among the glass samples. Additionally, the lowest HVL value should have the largest linear attenuation coefficient because of the inverse correlation between HVL and linear attenuation coefficient. The mean free path value was also studied as a part of the study of gamma-ray ab-sorption materials; this value, which represents the distance between the collision of an incoming particle with the particles within the shielding material, is an indicator of the material's ability to attenuate radiation by shifting its direction, and thus should be as small as possible. Absorption of an incoming photon is indicated by a low value of the mean free path when several interactions are carried out at close distances.

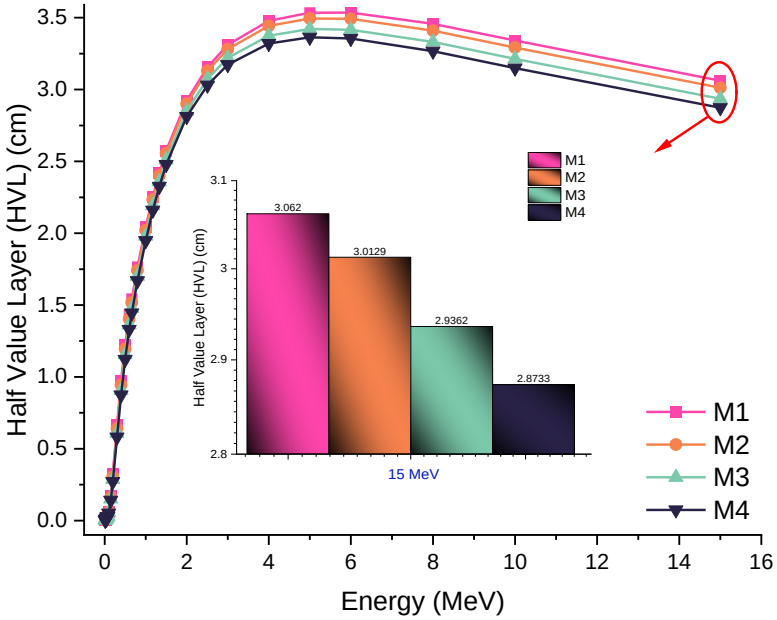

Figure 3. Variation of half-value layer (cm) with photon energy (MeV) for all M1–M4 glasses.

As seen in Figure 4, the M4 sample reported the lowest value of mean free path along with increasing the incident photon energy. This could be another illustration of the advantage of increasing the WO_3 composition in tellurite glass material. One critical component in gamma-ray absorption materials is the effective atomic number (Z_{eff}). In general, the more electrons a material has around its nucleus, the higher its Z number [23]. Because of the high probability of collision that may excite or drop an electron off its orbit, the energy of an incoming photon is reduced if it interacts with a nucleus with a high Z number because of the large number of electrons in its orbit.

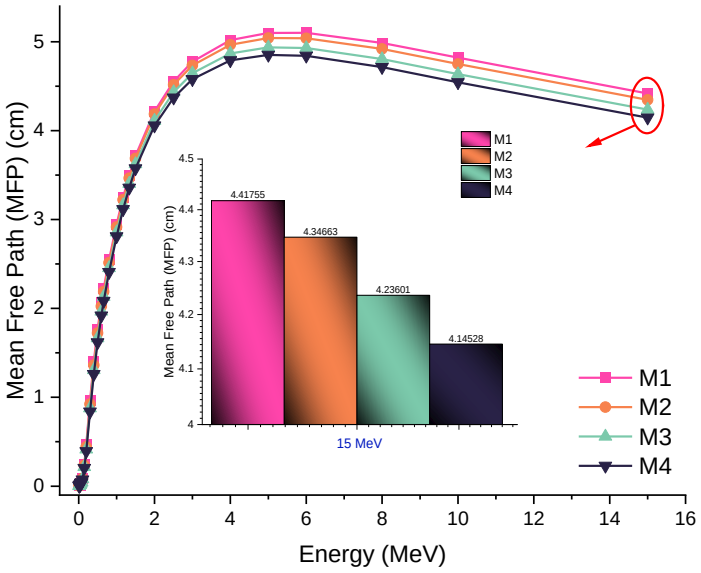

Figure 4. Variation of mean free path (cm) with photon energy (MeV) for all M1–M4 glasses.

The Z_{eff} vs. energy is shown in Figure 5. The high absorption process in the low energy ranges is reflected in the graph as high effective atomic numbers of the four glass material samples. As the energy increases, a steady drop in energy from 0.08 MeV to 1.5 MeV occurs, where the Compton scatter effect is more dominant, and increases back to the high energy range of 2–15 MeV. The M4 sample, with the highest WO_3 composition of 30 mol%, was

reported to have the highest effective atomic number among all glass samples. This was due to the high Z number of W, which shifted to the tellurite glass system.

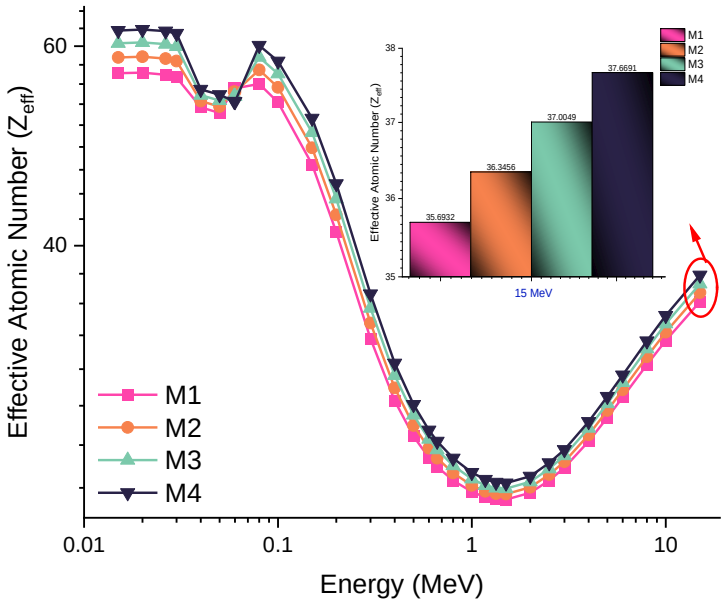

Figure 5. Variation of effective atomic number (Z_{eff}) with photon energy (MeV) for all M1–M4 glasses.

The effective electron density (N_{eff}) is illustrated in Figure 6, where variations of the four glass samples are shown through different ranges of energies. It is recognized that electrons play a fundamental role in interaction with matter. The M4 sample was reported to have the highest effective electron density of 6.8877 electrons/g at an energy of 0.03 MeV, where a decrease began as the energy started to increase with the Compton scattering effect. In addition, effective conductivity (C_{eff}) was examined for the four glass samples in Figure 7 with varying photon energies.

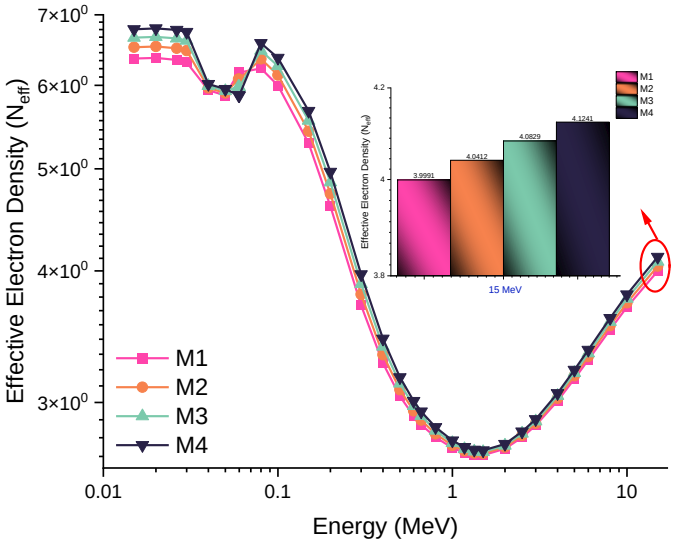

Figure 6. Variation of effective electron density (electrons/g) with photon energy (MeV) for all M1–M4 glasses.

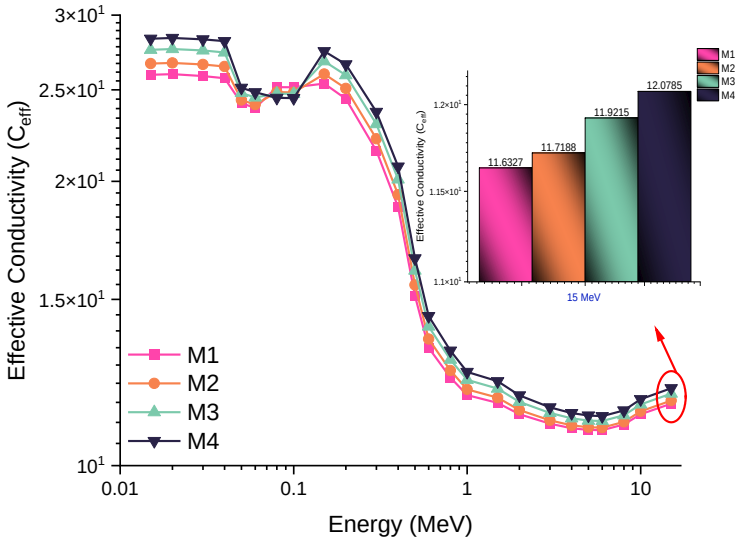

Figure 7. Variation of effective conductivity (C_{eff}) with photon energy (MeV) for all M1–M4 glasses.

A clear high C_{eff} was reported in low energy ranges, where a decrease b in the range of 0.03 MeV to 0.06 MeV. However, the M4 sample had the highest (C_{eff}) value among all samples in almost all energy ranges, which might be due to the addition of the high Z number element that contributed to the growing number of electrons. Overall, our examination of gamma-ray absorption properties was proven to be robust, where 30% composition of WO_3 in the tellurite glass system was found to achieve the optimum properties of absorbing gamma-ray materials among all tested glass materials. Figures 8 and 9 depict the variation in EBF and EABF values found for M1, M2, M3, and M4 glasses having different concentrations of TeO_2, WO_3, and GdF_3 across mfp values ranging from 0.5 to 40. It is clear from the graphs that the EBF and EABF levels were lowest at relatively low mfp values. A rapid increase in the primary photon's interaction rate occurred after it passed through the absorber [23]. Figures 8 and 9 show that compared to the glass sample consisting of 40% WO_3 and 0% GdF_3, the EBF and EABF values of the low WO_3 incorporation sample were much higher. It's well known that a higher interaction count indicates quick quantitative absorption. Low EBF and EABF values, both of which are important indicators for optimal photon-matter interaction within the absorber, indicate that M4 has the ideal composition for absorbing high-energy gamma rays. In the same examination, M4 had the maximum material density, with 40% WO_3 and 0% GdF_3 showed the maximum radiation shielding capabilities among the tested materials. Because of this, This sample could be used to protect against ionizing radiation and to dampen the effects of gamma rays. In general, the investigation we performed on the absorption characteristics of powerful photons showed that they are stable over time. The glass with a composition of 60 mol% TeO_2, 40 mol% WO_3, and 0 mol% GdF_3 (i.e., M4) was found to have the highest efficiency in absorbing gamma rays.

3.2. Elastic Moduli and Mechanical Properties

In this study, some of the critical mechanical parameters such as E(Young's), B(bulk), S(shear), L(longitudinal), H(micro-hardness) moduli and σ(Poisson's ratio) were calculated for the examined glasses at varying molar fractions of GdF_3 using the theoretical design suggested by Makishima-Mackenzie for multi-componenet glasses [24]. The utilized methodology mostly depends on packing density (Vi) and Gibbs free energy (G). The derived elastic moduli and Poisson's ratio are presented in Table 2. Using the calculated quantities, we describe and explain the assessed outcomes of the other elastico-mechanical parameters. The literature review showed that glass-ceramic, inorganic, organic, and metallic glasses are all evaluated for their strength using this fundamental physical property in materials physics [25,26]. It is important to note that this ratio also relies on other factors [27]. The glass ratio of Poisson for this system varies from 0.42740 to 0.43063 when

the GdF_3 molar percentage in the glasses changes from 0 to 30 mol%. Table 2 lists the thermodynamic-features of the glassy system that are concealed by the Gibbs free energy. This value ranges from 59.52 kJ/cm^3 at low GdF_3 mol% to 45.42 kJ/cm^3 at high GdF_3 mol%. This systematical linear reduction is coupled with a rise In sample density. These findings suggest that the thermodynamics of glass systems relies on physical characteristics that relate to the entire molecular structure of the glassy network, as contrasted to just one element or molecule, like the Poisson's ratio of glass systems, which rely on OMV-ODP. In addition, various moduli were shown to decrease linearly with the molar increase of GdF_3 in the glassy network's molecular structure. For instance, Young's modulus has a value of 62.23 GPa, which decreases to 45.37 GPa at low GdF_3 mol% and increases at high GdF_3 mol%. These elastic properties of these glasses were determined by the interatomic-bonding, coordination-number, and directional order value in the unit cell [28].

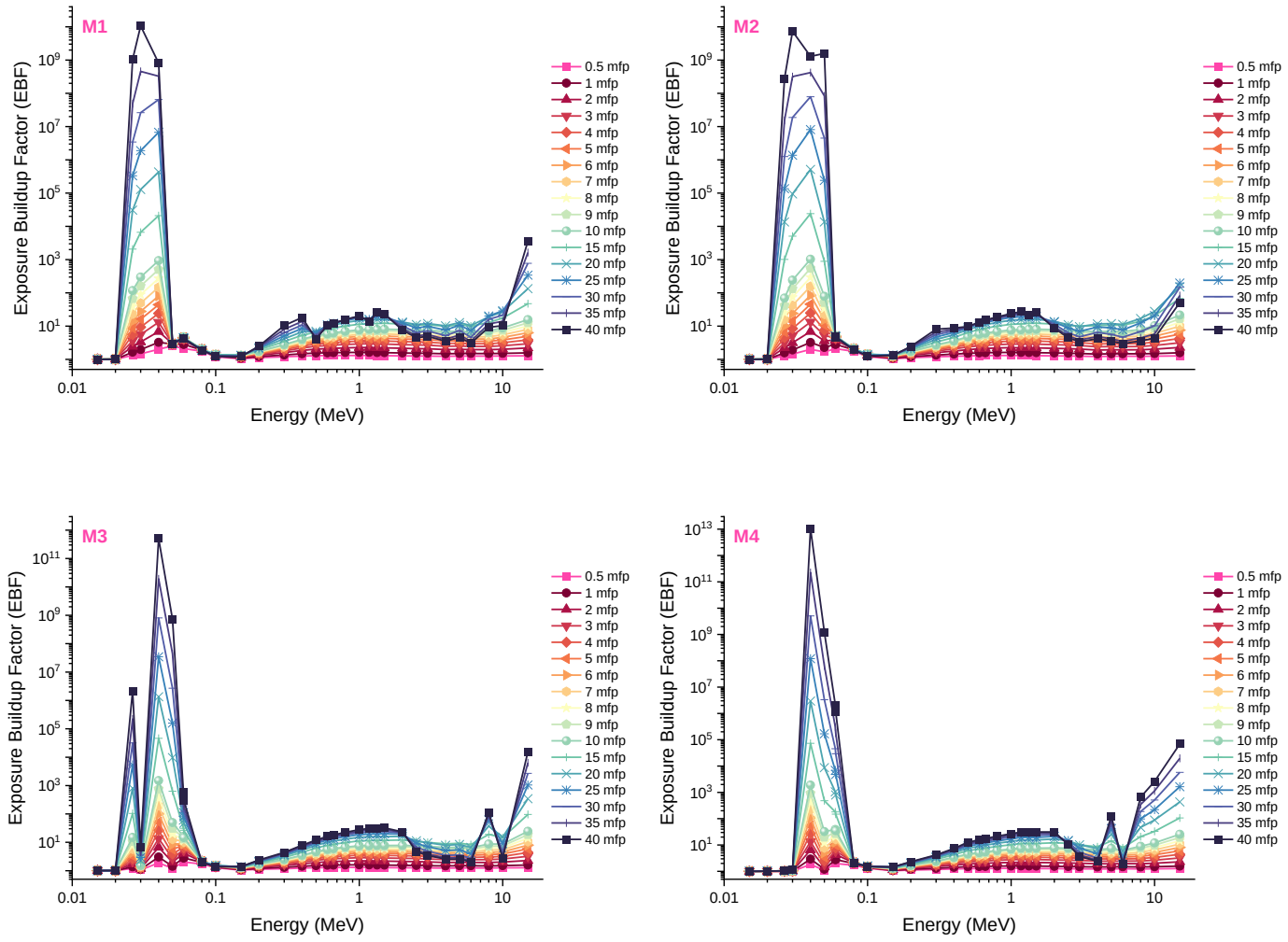

Figure 8. Variation of exposure buildup factors (EBF) of investigated glasses at different mean free path values.

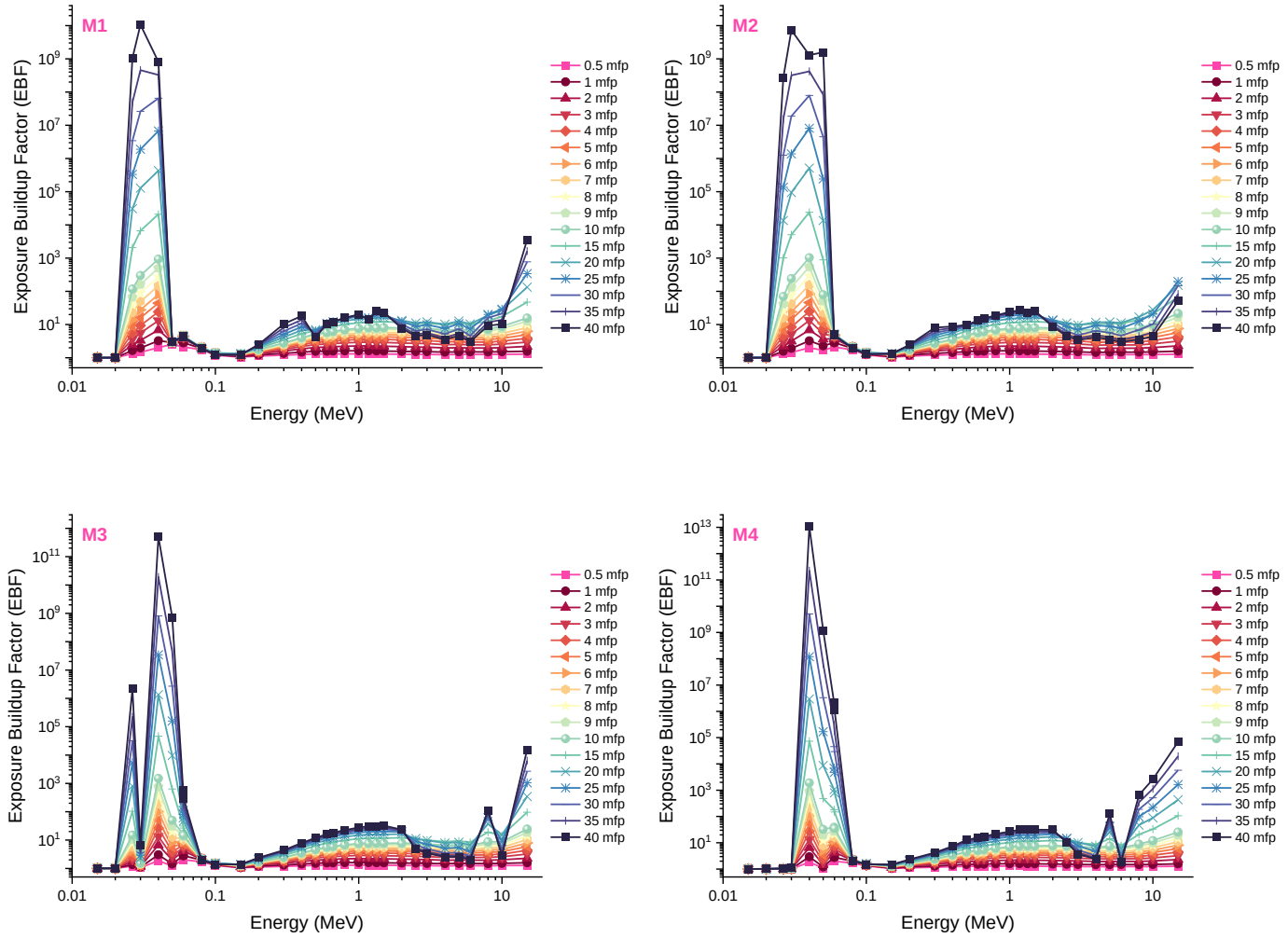

Figure 9. Variation of energy absorption buildup factors (EABF) of investigated glasses at different mean free path values.

Table 2. The mechanical parameters and elastic moduli of the investigated samples.

Sample Code	ΣV_i (cm^3/mol)	G (kJ/cm^3)	V_t (cm^3/mol)	E (GPa)	B (GPa)	S (GPa)	L (GPa)	σ	H (GPa)
M1	17.34	59.52	0.522732	62.226	39.033	25.207	57.938	0.42740	0.01695
M2	16.801	54.82	0.512684	56.211	34.582	22.867	51.732	0.42879	0.01661
M3	16.262	50.12	0.507303	50.852	30.957	20.735	46.508	0.42954	0.01643
M4	15.723	45.42	0.49948	45.373	27.195	18.566	41.120	0.43063	0.01616

4. Conclusions

The main goal was to evaluate the fundamental gamma-ray shielding and mechanical properties of a variety of tellurite glasses. Glass materials have been demonstrated to be a favorable shielding material against ionizing radiation, despite the limitations of typical shielding materials like lead and concrete. Among the many possibilities for protecting laboratories during scientific experiments, glass stands out as a non-hazardous and long-lasting option. Many researchers and engineers have taken use of this fact to employ glass in radiation shielding and optical applications. Glass samples, M1, M2, M3, and M4, were designed using a melt-quenching process and went under investigation for gamma-ray shielding properties with a broad range of incident photon energies. Each

sample with different composition resulted in distinct densities. The M4 sample, with 40% WO_3 and 60% TeO_2, stood out as having the greatest density among all tested samples with 5.8204 g/cm^3 in addition to other essential gamma-ray shielding parameters. Our investigation showed that M4 had the highest values of μ and MAC at most energy ranges among all glass samples, with a linear attenuation coefficient of 0.35579 and a MAC of 0.061128 at an energy of 1 MeV. The HVL value was measured as well through a range of photon energy levels. The M1, M2, M3, and M4 HVL values at an energy level of 0.4 MeV were reported as 0.9742 cm, 0.9437 cm, 0.906 cm, and 0.8739, respectively. M4, with the greatest WO_3 concentration, was the most efficient attenuating material with the lowest maximum thickness. Furthermore, with the large addition of WO_3 in the tellurite glass system, the M4 sample had the highest effective atomic number (Z_{eff}) by far among almost all energy levels, indicating the effective attenuating ability of gamma rays. Variations in effective electron density (electrons/g) and effective conductivity (C_{eff}) were measured at varied incoming photon energies. The M4 sample was the most prominent of all the evaluated glass samples, indicating a large number of electrons in a structure and high electron mobility. As a result, our robust investigation of gamma-ray absorption properties with different glass materials concluded that the M4 sample was by far the most outstanding sample in terms of radiation shielding ability. Furthermore, the large addition of WO_3 to a glass material was proven to provide advantages to the glass system that would make it more effective in absorbing different levels of energy and a promising alternative material in radiation shielding technology. The elastic moduli and Poisson's ratios (σ) of the studied glass at a different molar fractions of GdF_3 were evaluated utilizing the theoretical approach developed by Makishima–Mackenzie. Poisson's ratio (σ) increased, while all elastic moduli decreased. Although the findings of this research examine the gamma-ray absorption properties of tellur glasses in detail, they should be compared with those of traditional absorption materials by doing a cost analysis. This relates to the volumetric width in certain radiation areas and the possible shielding design costs associated with this size. Conventional materials, such as concrete, are simple to produce and access in terms of their structural components. This circumstance has made these materials the favored absorber materials around the world. The creation of this type of glass needs more technical infrastructure than the production of concrete. In terms of sustainable manufacturing, this is another crucial issue that must be addressed as a conclusion of the current investigation.

Author Contributions: Conceptualization, G.A. and H.O.T.; methodology, D.S.B. and H.O.T.; software, H.O.T., E.R., H.M.H.Z., Y.S.R., D.S.B. and A.E.; validation, E.I., G.K. and A.E.; formal analysis, H.M.H.Z. and D.S.B.; investigation, G.A. and H.O.T.; resources, Z.Y.K., E.I. and G.K.; data curation, G.A. and A.E.; writing—original draft preparation, Z.Y.K., E.R., A.E., H.O.T., Y.S.R. and G.K.; writing—review and editing, H.M.H.Z. and A.E.; visualization, G.A. and G.K.; supervision, Z.Y.K., Y.S.R., H.M.H.Z. and G.K.; project administration, A.E. and H.O.T.; funding acquisition A.E. (The author A.E. would like to thank "Dunarea de Jos" University of Galati, Romania, for the material and technical support). All authors have read and agreed to the published version of the manuscript.

Funding: Princess Nourah bint Abdulrahman University Researchers Supporting Project number (PNURSP2023R149), Princess Nourah bint Abdulrahman University, Riyadh, Saudi Arabia.

Data Availability Statement: Data are available upon reasonable request.

Acknowledgments: The authors would like to express their deepest gratitude to Princess Nourah bint Abdulrahman University Researchers Supporting Project number (PNURSP2023R149), Princess Nourah bint Abdulrahman University, Riyadh, Saudi Arabia.

Conflicts of Interest: The authors declare no conflict of interest.

References

1. Brodsky, A.; Kathren, R.L. Historical development of radiation safety practices in radiology. *Radiographics* **1989**, *9*, 1267–1275. [CrossRef]
2. Edison, P.; Chang, P.S.; Toh, G.H.; Lee, L.N.; Sanamandra, S.K.; Shah, V.A. Reducing radiation hazard opportunities in neonatal unit: Quality improvement in radiation safety practices. *BMJ Open Qual.* **2017**, *6*, e000128. [CrossRef]

3. Langie, S.A.; Koppen, G.; Desaulniers, D.; Al-Mulla, F.; Al-Temaimi, R.; Amedei, A.; Azqueta, A.; Bisson, W.H.; Brown, D.; Brunborg, G.; et al. Causes of genome instability: The effect of low dose chemical exposures in modern society. *Carcinogenesis* **2015**, *36* (Suppl. 1), S61–S88. [CrossRef]
4. Seymour, C.B.; Mothersill, C. Radiation-Induced Bystander Effects—Implications for Cancer. *Nat. Rev. Cancer* **2004**, *4*, 158–164. Available online: https://radiationeffects.org/wp-content/uploads/2015/08/Radiation-induced-bystander-effects.pdf (accessed on 12 January 2023.). [CrossRef]
5. Mateuca, R.; Lombaert, N.; Aka, P.V.; Decordier, I.; Kirsch-Volders, M. Chromosomal changes: Induction, detection methods and applicability in human biomonitoring. *Biochimie* **2006**, *88*, 1515–1531. [CrossRef] [PubMed]
6. Hickling, S.; Xiang, L.; Jones, K.C.; Parodi, K.; Assmann, W.; Avery, S.; Hobson, M.; El Naqa, I. Ionizing radiation-induced acoustics for radiotherapy and diagnostic radiology applications. *Med. Phys.* **2018**, *45*, e707–e721. [CrossRef] [PubMed]
7. Pereira, G.C.; Traughber, M.; Muzic, R.F. The role of imaging in radiation therapy planning: Past, present, and future. *BioMed Res. Inter.* **2014**, *2014*, 231090. [CrossRef]
8. Holmberg, O.; Malone, J.; Rehani, M.; McLean, D.; Czarwinski, R. Current issues and actions in radiation protection of patients. *Eur. J. Radiol.* **2010**, *76*, 15–19. [CrossRef] [PubMed]
9. Finnerty, M.; Brennan, P.C. Protective aprons in imaging departments: Manufacturer stated lead equivalence values require validation. *Eur. Radiol.* **2005**, *15*, 1477–1484. [CrossRef] [PubMed]
10. Ngaile, J.E.; Uiso, C.B.S.; Msaki, P.; Kazema, R. Use of lead shields for radiation protection of superficial organs in patients undergoing head CT examinations. *Radiat. Prot. Dosim.* **2008**, *130*, 490–498. [CrossRef]
11. AbuAlRoos, N.J.; Amin, N.A.B.; Zainon, R. Conventional and new lead-free radiation shielding materials for radiation protection in nuclear medicine: A review. *Radiat. Phys. Chem.* **2019**, *165*, 108439. [CrossRef]
12. Kang, J.H.; Oh, S.H.; Oh, J.I.; Kim, S.H.; Choi, Y.S.; Hwang, E.H. Protection evaluation of non-lead radiation-shielding fabric: Preliminary exposure-dose study. *Oral Radiol.* **2019**, *35*, 224–229. [CrossRef] [PubMed]
13. Tishkevich, D.I.; Grabchikov, S.S.; Lastovskii, S.B.; Trukhanov, S.V.; Vasin, D.S.; Zubar, T.I.; Kozlovskiy, A.L.; Zdorovets, M.V.; Sivakov, V.A.; Muradyan, T.R.; et al. Function composites materials for shielding applications: Correlation between phase separation and attenuation properties. *J. Alloys Compd.* **2019**, *771*, 238–245. [CrossRef]
14. Kilic, G.; Ilik, E.; Issa, S.A.; ALMisned, G.; Tekin, H.O. Tailoring critical material properties of some ternary glasses through ZnO/CdO alteration: A focusing study on multiple behavioral changes. *Appl. Phys. A* **2022**, *128*, 890. [CrossRef]
15. El-Mallawany, R.; Abdalla, M.D.; Ahmed, I.A. New tellurite glass: Optical properties. *Mater. Chem. Phys.* **2008**, *109*, 291–296. [CrossRef]
16. Zhang, X.; Zhang, J.; Zhou, C.; Sun, Y.; Li, P.; Qi, X. High refractive index of Eu^{3+} doped La_2O_3-TiO_2-Nb_2O_5-WO_3 oxide glasses with low wavelength dispersion. *J. Non-Cryst. Solids* **2022**, *581*, 121228. [CrossRef]
17. Shoaib, M.; Rooh, G.; Chanthima, N.; Sareein, T.; Kim, H.J.; Kothan, S.; Kaewkhao, J. Luminescence behavior of Nd^{3+} ions doped ZnO-BaO-(Gd_2O_3/GdF_3)-P_2O_5 glasses for laser material applications. *J. Lumin.* **2021**, *236*, 118139. [CrossRef]
18. Li, C.; Zhang, X.; Onah, V.C.; Yang, W.; Leng, Z.; Han, K.; Zhang, F.; Zhang, Y.; Han, Y.; Li, Y.; et al. Physical and optical properties of TeO_2-WO_3-GdF_3 tellurite glass system. *Ceram. Int.* **2022**, *48*, 12497–12505. [CrossRef]
19. Cheewasukhanont, W.; Limkitjaroenporn, P.; Sayyed, M.I.; Kothan, S.; Kim, H.J.; Kaewkhao, J. High density of tungsten gadolinium borate glasses for radiation shielding material: Effect of WO_3 concentration. *Radiat. Phys. Chem.* **2022**, *192*, 109926. [CrossRef]
20. Mann, K.S.; Mann, S.S. Py-MLBUF: Development of an online-platform for gamma-ray shielding calculations and investigations. *Ann. Nucl. Energy* **2021**, *150*, 107845. [CrossRef]
21. Celen, Y.Y.; Sarihan, M.; Almisned, G.; Tekin, H.O.; Ekmekçi, I. Calculation of gamma-ray buildup factors for some medical materials. *Emerg. Mater. Res.* **2022**, *11*, 388–398. [CrossRef]
22. Tekin, H.O.; ALMisned, G.; Issa, S.A.; Zakaly, H.M. A rapid and direct method for half value layer calculations for nuclear safety studies using MCNPX Monte Carlo code. *Nucl. Eng. Technol.* **2022**, *54*, 3317–3323. [CrossRef]
23. Ilik, E. Effect of heavy rare-earth element oxides on physical, optical and gamma-ray protection abilities of zinc-borate glasses. *Appl. Phys. A* **2022**, *128*, 496. [CrossRef]
24. Makishima, A.; Mackenzie, J.D. Direct Calculation of Young's Modulus of Glass. *J. Non-Cryst. Solids* **1973**, *12*, 35–45. [CrossRef]
25. Rouxel, T. Elastic properties and short-to medium-range order in glasses. *J. Am. Ceram. Soc.* **2007**, *90*, 3019–3039. [CrossRef]
26. To, T.; Jensen, L.R.; Smedskjaer, M.M. On the relation between fracture toughness and crack resistance in oxide glasses. *J. Non-Cryst. Solids* **2020**, *534*, 119946. [CrossRef]
27. Ghosh, S.; Sharma, A.D.; Mukhopadhyay, A.K.; Kundu, P.; Basu, R.N. Effect of BaO addition on magnesium lanthanum alumino borosilicate-based glass-ceramic sealant for anode-supported solid oxide fuel cell. *Int. J. Hydrogen Energy* **2010**, *35*, 272–283. [CrossRef]
28. Lawrance, G.A. *Introduction to Coordination Chemistry*; John Wiley & Sons, Ltd.: Hoboken, NJ, USA, 2009.